

The spherical deformation model

ASGER HOBOLTH

*Department of Mathematical Sciences, University of Aarhus, Ny Munkegade, 8000 Aarhus C,
Denmark
asho@imf.au.dk*

SUMMARY

Miller *et al.* (1994) describe a model for representing spatial objects with no obvious landmarks. Each object is represented by a global translation and a normal deformation of a sphere. The normal deformation is defined via the orthonormal spherical-harmonic basis. In this paper we analyse the spherical deformation model in detail and describe how it may be used to summarize the shape of star-shaped three-dimensional objects with few parameters. It is of interest to make statistical inference about the three-dimensional shape parameters from continuous observations of the surface and from a single central section of the object. We use maximum-likelihood-based inference for this purpose and demonstrate the suggested methods on real data.

Keywords: Deformable templates; Shape; Spherical harmonic; Stationarity.

1. INTRODUCTION

Miller *et al.* (1994) describe a model for representing three-dimensional amoebae in optical sectioning microscopy. Each amoeba is represented by a global translation and a normal deformation of a sphere. The Gaussian model for the normal deformation is defined via the spherical-harmonic basis and possesses rotational symmetry. The purpose of this paper is to give a more detailed investigation of the spherical deformation model, and to use the model to explore shape variability. Here shape refers to the geometrical properties of an object which are invariant under translation, rotation and isotropic scaling.

Shape modelling of planar objects with no obvious landmarks has attracted much attention recently. Grenander and Miller (1994) propose a model where a planar object is represented by n vertices around its perimeter, and is described by deforming an n -sided regular polygon using edge transformations. The edge model of Grenander and Miller (1994) is analysed in detail in Kent *et al.* (2000), who use the model to explore shape variability. In Hobolth *et al.* (2002) the object is described using vertex transformations, and it is concluded that Fourier analysis of the standardized radius-vector function is an efficient way of exploring shape variability for star-shaped planar objects. In this paper the three-dimensional spherical counterpart of the planar circulant Fourier analysis is investigated. It is also demonstrated how to perform statistical inference about the three-dimensional shape parameters from central sections of the object. This possibility is of great practical importance since it is usually much easier to obtain one digital image of the central section of an object than obtaining the whole surface.

The objects considered in this paper are neurons from the human hippocampus. The number of neurons in the human hippocampus decrease during normal aging (West, 1994) and Alzheimers dementia (West *et al.*, 1994). Similarly it is believed that the shape distribution of neurons in the human hippocampus changes during age and diseases such as ischemia, Alzheimers dementia, etc. A quantitative description



Fig. 1. Surfaces of five neurons from the human hippocampus.



Fig. 2. Central sections of ten neurons from the human hippocampus.

of the architecture of neurons in the human hippocampus may be found in Amaral and Witter (1989). Cell shape changes are also believed to take place during various types of cancer. In the biological literature Fourier descriptors are commonly used to quantify planar shapes: see, for example Lestrel (1997) and references therein. The spherical deformation model provides a stochastic extension to three-dimensional space of the planar Fourier descriptors.

The paper is organized as follows. In Section 2 the two samples of data are described. The first data sample consists of the surfaces of five neurons from the human hippocampus, the second consists of ten central sections of neurons from the human hippocampus. Section 3 is concerned with the geometry of the spherical-harmonic basis. In Section 4 the spherical deformation model is specified, and in Section 5 the model is fitted to the five surfaces of neurons from the human hippocampus. The relation between the circulant and the spherical models is outlined in Section 6, and in Section 7 the relation is used to fit the spherical deformation model to the ten central sections of neurons from the human hippocampus. The paper concludes with a discussion on the use of the spherical deformation model.

2. THE DATA

Optical sectioning microscopy (OSM) is a widely used tool to get access to the 3D structure of biological specimens. In OSM a series of focal planes spanning the specimen are acquired. This paper is devoted to the study of neurons from the human hippocampus. The hippocampus is the part of the brain concerned with recent memory and the ability to learn new facts and skills. A hippocampus neuron can be viewed as a small deformation of a sphere with a typical diameter of 10–15 μm . The focal planes of a 70 μm thick glycol methacrylate section were viewed in an Olympus BX 50 light microscope. The microscope was mounted with a 100X oil objective with a small focal depth (NA 1.4), a motorized microscope stage, and a 3 CCD video camera connected to a personal computer. From a specimen of one human hippocampus we collected the images of five neurons where the focal planes were 0.5 μm apart, and the magnification was chosen so that the central section of each neuron had a diameter of around 400 pixels. The central section was defined as the focal depth half-way from the top to the bottom of the neuron. Due to the substantial amount of optical distortion the boundary of each neuron was traced manually when the focal depth was at the top or bottom of the neuron whereas a simple thresholding was sufficient to obtain the boundary at the remaining focal depths. We also collected the boundary of the central section of ten neurons. The data from the 15 randomly chosen neurons are shown in Figures 1 and 2.

3. SPHERICAL HARMONICS

Consider a solid object $K \subset \mathbb{R}^3$ and suppose that K is star-shaped relative to $z \in K$, i.e. every point on the surface of K is visible from z . Using spherical coordinates the surface is determined by

$$\{z + r(\theta, \phi)\omega(\theta, \phi) : 0 \leq \theta < 2\pi, 0 \leq \phi \leq \pi\},$$

where $\omega(\theta, \phi) = (\cos\theta \sin \phi, \sin\theta \sin \phi, \cos\phi)$ is the vector on the unit sphere with polar longitude θ and polar latitude ϕ , and $r(\theta, \phi)$ is the distance from z to the surface of K in the direction $\omega(\theta, \phi)$. It is useful to express the radius-vector function $r(\theta, \phi)$ in terms of the spherical harmonics

$$\{\varphi_n^m(\theta, \phi) : n \in \mathbb{N}_0, m = -n, \dots, n\},$$

which constitute an orthonormal basis on the sphere. The spherical harmonics are given by

$$\varphi_n^m(\theta, \phi) = \begin{cases} k_n^{|m|} P_n^{|m|}(\cos\phi) \cos m\theta, & m = -n, \dots, -1 \\ k_n^0 P_n^0(\cos\phi), & m = 0 \\ k_n^m P_n^m(\cos\phi) \sin m\theta, & m = 1, \dots, n, \end{cases}$$

where

$$k_0^0 = \frac{1}{\sqrt{2\pi}}, k_n^0 = \sqrt{\frac{2n+1}{4\pi}}, k_n^m = \sqrt{\frac{2n+1}{2\pi} \frac{(n-m)!}{(n+m)!}}, n \in \mathbb{N}, m = 1, \dots, n, \tag{3.1}$$

are normalizing constants and P_n^m are the associated Legendre functions of the first kind.

Now consider the Fourier–Legendre series expansion

$$r(\theta, \phi) = \sum_{n=0}^{\infty} \sum_{m=-n}^n a_n^m \varphi_n^m(\theta, \phi)$$

of the radius-vector function, where the Fourier–Legendre coefficients are given by

$$a_n^m = \int_0^{2\pi} \int_0^\pi r(\theta, \phi) \varphi_n^m(\theta, \phi) \sin \phi \, d\phi \, d\theta. \tag{3.2}$$

The mean radius-vector length is determined by

$$\bar{r} = \frac{1}{4\pi} \int_0^{2\pi} \int_0^\pi r(\theta, \phi) \sin \phi \, d\phi \, d\theta = \frac{1}{\sqrt{2\pi}} a_0^0,$$

hence a_0^0 can be used as a measure of the size of the object. To remove size one may consider the standardized radius-vector function $r(\theta, \phi)/\bar{r}$.

The choice of centre implies constraints on the radius-vector function. If z is the centre of mass of the object then the constraints can be written explicitly, as shown in the Appendix. In this case the constraints involve the fourth power of the radius-vector function, but assuming that the object is a small deformation of a sphere, a first-order Taylor expansion leads to the approximate constraints $a_1^m \approx 0, m = -1, 0, 1$.

To understand the geometry of the Fourier–Legendre coefficients a_n^m with index $n \geq 2$ it is useful to consider objects given by

$$r(\theta, \phi) = 1 + a_n^m \varphi_n^m(\theta, \phi). \tag{3.3}$$

In general these objects are quite complicated. An example is given in Figure 3.

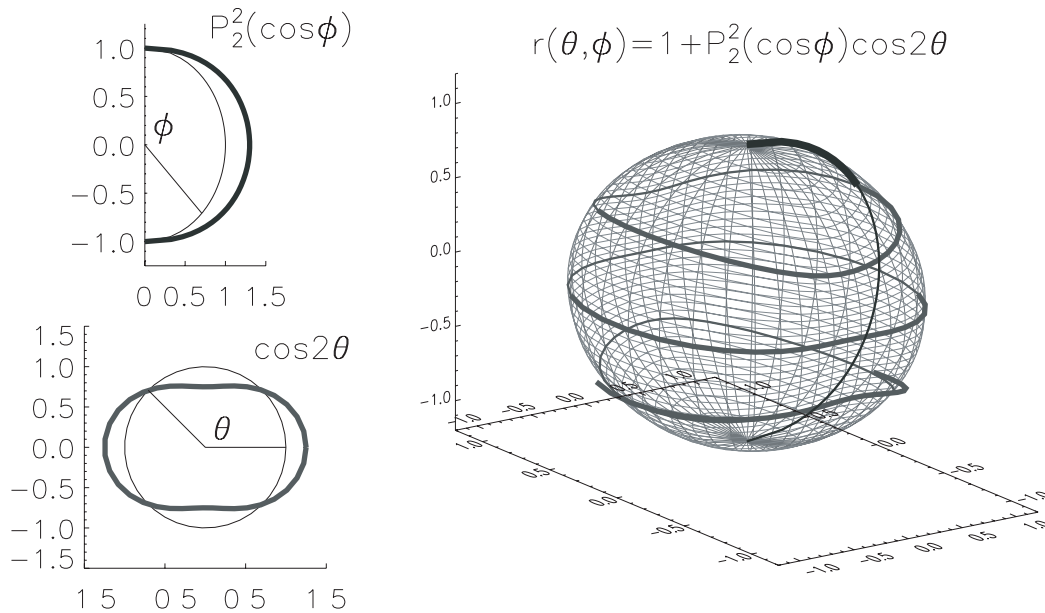


Fig. 3. Illustration of the geometry of an object given by (3.3) with $m = -2$ and $n = 2$. To the left the Legendre function $P_2^2(\cos\phi)$, $0 \leq \phi \leq \pi$, and the trigonometric function $\cos 2\theta$, $0 \leq \theta < 2\pi$, are wrapped around the semicircle and the circle. To the right the resulting surface is shown. The four accentuated curves correspond to fixed $\phi = \pi/2, \pi, 3\pi/2$ and $\theta = 0$.

4. THE SPHERICAL DEFORMATION MODEL

Consider the Fourier–Legendre series expansion of the standardized radius-vector function

$$r(\theta, \phi) = 1 + \sum_{n=1}^{\infty} \sum_{m=-n}^n a_n^m \phi_n^m(\theta, \phi).$$

As argued in the previous section the three Fourier–Legendre coefficients corresponding to $n = 1$ are approximately zero if z is the centre of mass and the object is a small deformation of a sphere. Alternatively one could choose the centre as the point satisfying $a_1^m = 0$, $m = -1, 0, 1$ (assuming the object is star-shaped relative to this point). In any case these coefficients are treated as non-random nuisance parameters. The remaining coefficients

$$a_n^m \sim N(0, \lambda_n^m), \quad n \geq 2, \quad m = -n, \dots, n,$$

are modelled as independent Gaussian random variables with mean zero (the average shape is a sphere) and variance λ_n^m . We also suppose that we have *stationarity on the sphere*, in the sense that the covariance between two points on the sphere depends only on the angle between the points. Stationarity is obtained by assuming

$$\lambda_n^m = \lambda_n, \quad n \geq 2, \quad m = -n, \dots, n, \tag{4.1}$$

and the covariance becomes

$$\begin{aligned} \text{Cov}(r(\theta_1, \phi_1), r(\theta_2, \phi_2)) &= \sum_{n=2}^{\infty} \lambda_n \sum_{m=-n}^n \varphi_n^m(\theta_1, \phi_1) \varphi_n^m(\theta_2, \phi_2) \\ &= \sum_{n=2}^{\infty} \lambda_n (k_n^0)^2 P_n(\cos \psi_{12}), \end{aligned} \tag{4.2}$$

where $\cos \psi_{12} = \omega(\theta_1, \phi_1) \cdot \omega(\theta_2, \phi_2)$, and the second equality uses the *addition theorem*, (cf. Müller, 1966, Theorem 2).

The covariance is thus determined by the variances λ_n . To proceed further we seek a parametric model for the variances. Miller *et al.* (1994) use a model induced from Poisson’s equation for pressure fields acting on thin membranes, with associated potential

$$E(r) = \frac{1}{2} \int_0^{2\pi} \int_0^\pi |Lr(\theta, \phi)|^2 \sin \phi \, d\phi \, d\theta,$$

where

$$L = \frac{\partial^2}{\partial \theta^2} + \frac{\cos \theta}{\sin \theta} \frac{\partial}{\partial \theta} + \frac{1}{\sin^2 \theta} \frac{\partial^2}{\partial \phi^2}$$

is the Laplacian operator on the surface of the sphere. Since $\varphi_n^m(\theta, \phi)$ is an eigenfunction of the Laplacian operator with eigenvalue $\eta_n = -n(n + 1)$ this potential corresponds to a model in which the variances decrease as $1/\lambda_n = \eta_n^2 = (n(n + 1))^2$.

Grenander and Miller (1998, Section 5.3) suggest obtaining more general models by introducing polynomials $p(L) = a_0I + a_1L + \dots + a_dL^d$ of the basic operator L . The bi-harmonic operator is for example obtained by choosing $p(L) = L^2$. For such models the variances decrease as $1/\lambda_n = p(\eta_n)^2$.

In this paper we suggest letting the variances decrease according to

$$1/\lambda_n = \alpha + \beta n^p, \quad n \geq 2, \quad p > 2, \quad \beta > 0, \quad \alpha > -\beta \times 2^p. \tag{4.3}$$

There are several reasons why we believe this is a good model. The parameter p makes the model very flexible with regard to the smoothness of the radius-vector function. From Stein (1999, Chapter 2) it follows that the degree of mean square differentiability is determined by the behaviour of the covariance function and its derivatives near the origin. By making repeated use of the relation

$$P'_{n+1}(x) = (2n + 1)P_n(x) + P'_{n-1}(x), \quad -1 \leq x \leq 1,$$

and using $P_0(x) = 1$, $P_1(x) = x$ and $P_n(1) = 1$ it can be shown that the radius-vector function is k times mean square differentiable when $2(k + 1) < p \leq 2(k + 2)$. When $2 < p \leq 4$ the radius-vector function is mean square continuous. Note that in the model used by Miller *et al.* (1994) the variances decrease according to $p = 4$, while for the bi-harmonic operator the variances decrease according to $p = 8$.

For fixed p the value of β determines the ‘local’ shape of the object since the variances with large indices are determined by β . The third parameter in the model is most easily interpreted by making the reparametrization $\tilde{\alpha} = \alpha + \beta \times 2^p$, in which case $\tilde{\alpha}$ controls the first few variances and thereby the ‘global’ shape of the object. In Figure 4 simulations of central sections $\{r(\theta, \pi/2) : 0 \leq \theta < 2\pi\}$ from the model (4.3) with fixed $p = 4$ and varying $\tilde{\alpha}$ and β are shown.

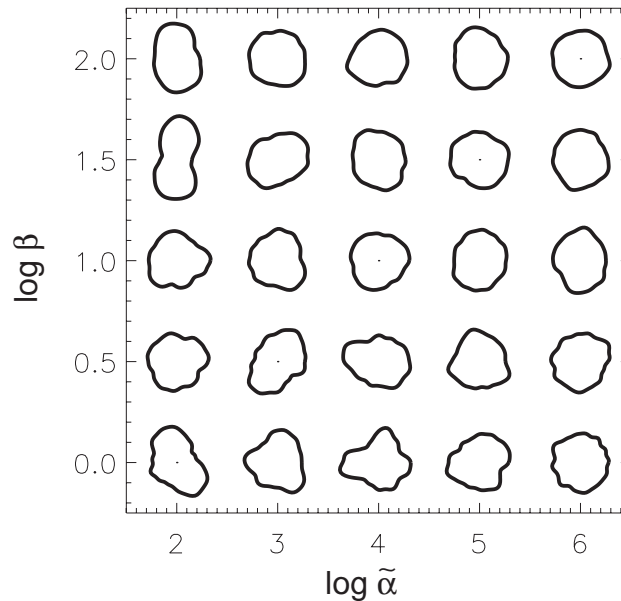


Fig. 4. Simulated central sections under the model (4.3) with $p = 4$ and indicated values of $\tilde{\alpha}$ and β .

5. APPLICATION I: OBSERVING THE WHOLE SURFACE

Statistical inference in the spherical deformation model is straightforward when the observations of the object take the form of (approximately) continuous measurements of the radius-vector function. The data from Figure 1 are used to illustrate the methods. As explained in Section 2 we begin by tracing the boundary of the neuron in each section and thus represent the neuron by a binary volume (1 for a neuron voxel and 0 for a background voxel). From the centre of mass of the neuron equally spaced radii (in terms of ϕ and θ) are traced to the boundary. A boundary point is defined as the voxel location just before the first zero is obtained. The number of boundary points on the object chosen should be high enough to capture the shape of the neuron, but since the neuron is only represented as a binary volume not much extra information is gained by choosing a very high number.

The Fourier–Legendre coefficients $a_{n,k}^m$ for each neuron $k = 1, \dots, 5 = K$ are obtained from discrete versions of the integrals in (3.2) where the standardized radius-vector function is used. The variances $\lambda_{n,k}$ are calculated from the Fourier–Legendre coefficients

$$\hat{\lambda}_{n,k} = \frac{1}{2n+1} \sum_{m=-n}^n (a_{n,k}^m)^2 \sim \lambda_{n,k} \chi^2(2n+1)/(2n+1), \quad n \geq 2.$$

In the left-hand plot of Figure 5 the estimated log-variances are displayed for each of the five surfaces. Suppose the objects are independent and identically distributed (i.i.d.). Then the common variances λ_n are estimated by averaging the variances of the single neurons

$$\hat{\lambda}_n = \frac{1}{K} \sum_{k=1}^K \hat{\lambda}_{n,k} \sim \lambda_n \chi^2((2n+1)K)/((2n+1)K), \quad n \geq 2.$$

The estimated log-variances under the i.i.d. assumption are displayed in the right-hand plot of Figure 5.

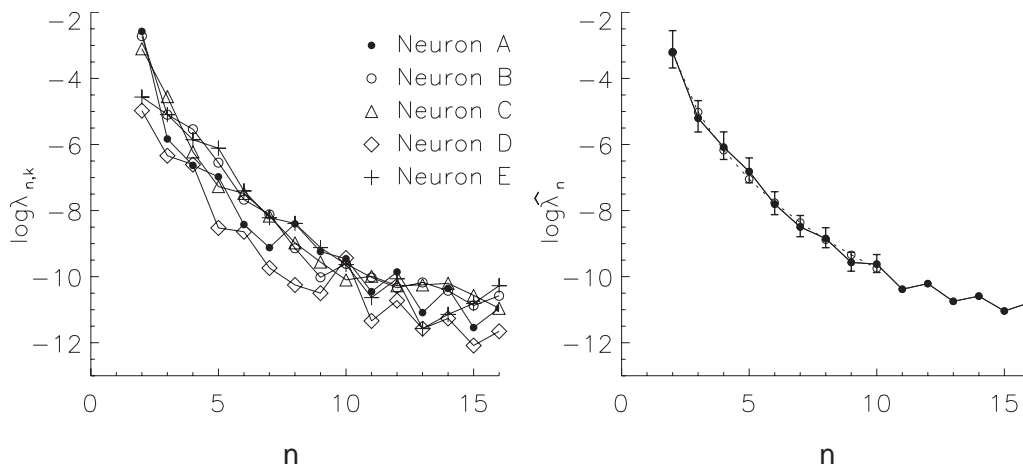


Fig. 5. Left: Estimated log-variances of the stationary model (4.1) for each of the five 3D surfaces. Letter A refers to the left-most surface in Figure 1, B to the second left-most surface etc. Right: Estimated log-variances of the stationary model (4.1; solid line) and the regression model (4.3; dotted line) for the 3D surfaces under an i.i.d. assumption. The error bars show the 95% confidence intervals under the stationary model.

In order to avoid effects due to the discretization of the neurons we choose to proceed with variances $\lambda_{n,k}$ of indices less than $n^* = 10$ only. The variances with indices above n^* are judged as being too noisy, as discussed below. The cutting off of the high-frequency components in the spectrum is well known in time series analysis, where it is referred to as low-pass filtering since only the low-frequency components are used for subsequent analysis. The (correspondingly truncated) regression model (4.3) is fitted to the variances $\hat{\lambda}_2, \dots, \hat{\lambda}_{n^*}$ using maximum likelihood. The maximum likelihood estimates of $(\tilde{\alpha}, \beta, p)$ are (24.9, 2.2, 3.9), and the right-hand plot of Figure 5 displays the log-variances under the fitted model. Carrying out a goodness of fit test of the (truncated) model (4.3) under the (truncated) model (4.1) assuming stationarity we obtain a likelihood ratio test statistic equal to 6.4 on $(n^* - 1) - 3 = 6$ degrees of freedom. Under the $\chi^2(6)$ approximation of the test statistic the ‘ p -value’ is 0.38, indicating that the model (4.3) gives a reasonable description of the decreasing variances. Based on the observed information matrix, an approximate 95% confidence interval for $\tilde{\alpha}$ is [11.2, 38.6], for β the interval is [0.7, 3.7] and for p it is [3.6, 4.2]. As expected, there are small correlations between the estimates of $\tilde{\alpha}$ and β (-0.14) and between $\tilde{\alpha}$ and p (0.13), but a very strong negative correlation between β and p (-0.98). Fixing $p = 4$ only changes the estimates of $\tilde{\alpha}$ and β slightly. Furthermore, the confidence interval for $\tilde{\alpha}$ remains almost unchanged while the confidence interval of β narrows to [1.9, 2.5].

In order to investigate the model assumptions and the digitization effects we conducted a simulation study. The surfaces of five objects are simulated according to the regression model (4.3) with $p = 4$ and the maximum likelihood estimates of (α, β) . Comparing the simulated spectra, shown in Figure 6, with the observed spectra in Figure 5, it does seem that there is more variation in the observed variances than in the simulated variances. This observation is investigated in more detail by performing a series of Bartlett tests for equal variances for each n . For $n = 5, 7$ and 8 the ‘ p -values’ of the tests were just below the 5% significance level and thus reject the hypothesis of equal variances. As is evident from Figure 5 the rejection is mainly due to the low variances of neuron B. In conclusion, there does seem to be more variability in the observed spectra than can be explained by the model, but it does not seem unreasonable to proceed with the i.i.d. assumption. More neurons are needed to obtain a clear decision on the validity of the i.i.d. assumption.

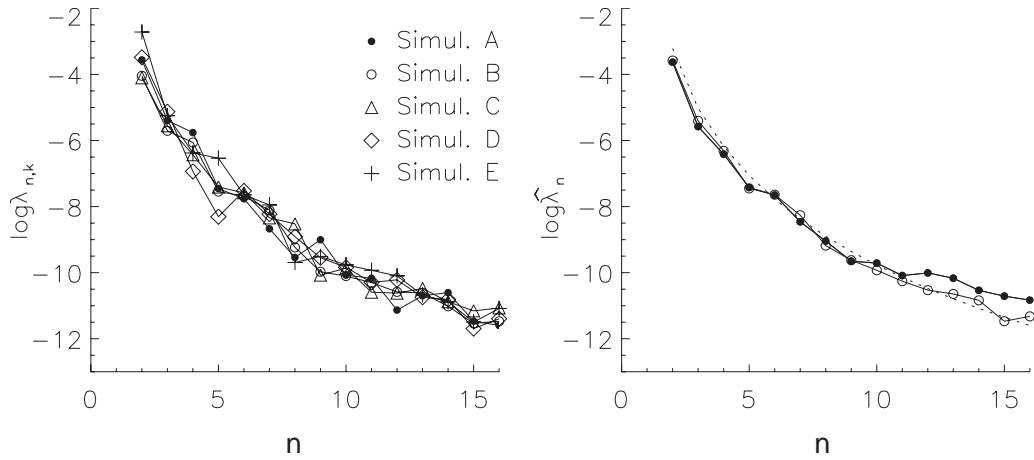


Fig. 6. Left: Spectra of five simulated surfaces under the regression model (4.3). Right: Estimated average spectrum of the five simulated surfaces before (open circles) and after (closed circles) digitization. The dotted line shows the log-variances under the regression model.

The effect on the spectra imposed by image resolution is explored by first representing the simulated surfaces as binary volumes with the same dimensions as the observed surfaces, then estimating the spectra of the binary volumes in the same manner as for the neurons. The result is shown in the right-hand plot of Figure 6. It seems that $n^* = 10$ is a good compromise which retains the structure in the low frequencies but does not result in the model fits being affected by the high-frequency variability, which is subject to digitization effects.

6. RELATION TO THE CIRCULAR DEFORMATION MODEL

Suppose we want to estimate the spherical variances λ_n of (4.1) from continuous measurements of the central sections

$$\{r(\theta, \pi/2) : 0 \leq \theta < 2\pi\}$$

only. This task is of considerable interest since the optical distortion complicates the reconstruction of the boundary at the top and bottom of the neurons. Furthermore, it is usually much easier to obtain one digital image of the central section of an object than to obtain the whole surface.

Whereas the spherical harmonics constitute the orthonormal basis on the sphere, the most convenient orthonormal basis on the circle is the Fourier basis

$$\left\{ \frac{1}{\sqrt{2\pi}}, \frac{1}{\sqrt{\pi}} \cos n\theta, \frac{1}{\sqrt{\pi}} \sin n\theta : n \in \mathbb{N} \right\}.$$

Similarly to the spherical case we can write the radius-vector function in terms of the Fourier basis

$$r(\theta, \pi/2) = \frac{b_0}{\sqrt{2\pi}} + \sum_{n=1}^{\infty} \left(b_n^c \frac{1}{\sqrt{\pi}} \cos n\theta + b_n^s \frac{1}{\sqrt{\pi}} \sin n\theta \right),$$

where the Fourier coefficients are given by

$$\begin{aligned}
 b_0 &= \int_0^{2\pi} r(\theta, \pi/2) \frac{1}{\sqrt{2\pi}} d\theta, \\
 b_n^c &= \int_0^{2\pi} r(\theta, \pi/2) \frac{1}{\sqrt{\pi}} \cos n\theta d\theta, \quad b_n^s = \int_0^{2\pi} r(\theta, \pi/2) \frac{1}{\sqrt{\pi}} \sin n\theta d\theta, \quad n \in \mathbb{N}.
 \end{aligned}
 \tag{6.1}$$

As in Section 2 we remove size by considering the standardized radius-vector function $r(\theta, \pi/2)/\bar{r}_{\pi/2}$, where

$$\bar{r}_{\pi/2} = \frac{1}{2\pi} \int_0^{2\pi} r(\theta, \pi/2) d\theta = \frac{1}{\sqrt{2\pi}} b_0.$$

Furthermore, the choice of centre implies constraints on the radius-vector function. As in 3D, the centre could be chosen as the point fulfilling $b_1^c = b_1^s = 0$. Another possibility is to choose the centre of mass in which case we have $b_1^c \approx 0$ and $b_1^s \approx 0$, provided that the central section is a small deformation of a circle. The last result is derived in the appendix of Hobolth *et al.* (2003), where a careful treatment of the geometry of the radius-vector function in the plane can also be found.

We now determine the distribution of the remaining Fourier coefficients. From

$$\begin{aligned}
 b_n^s &= \int_0^{2\pi} r(\theta, \pi/2) \frac{1}{\sqrt{\pi}} \sin n\theta d\theta = \int_0^{2\pi} \sum_{l=0}^{\infty} \sum_{m=-l}^l a_l^m \varphi_l^m(\theta, \pi/2) \frac{1}{\sqrt{\pi}} \sin n\theta d\theta \\
 &= \sqrt{\pi} \sum_{l=n}^{\infty} k_l^n P_l^n(0) a_l^n \sim N\left(0, \pi \sum_{l=n}^{\infty} (k_l^n P_l^n(0))^2 \lambda_l^n\right), \quad n \geq 2,
 \end{aligned}$$

and a similar calculation of b_n^c it follows that if we assume stationarity on the sphere (4.1) then the variances of b_n^c and b_n^s are equal and given by

$$\kappa_n = \sum_{l=n}^{\infty} \frac{2l+1}{2} \frac{(l-n)!}{(l+n)!} P_l^n(0)^2 \lambda_l, \quad n \geq 2.
 \tag{6.2}$$

Note that the relation between the circular variances κ_n and the spherical variances λ_n is linear. Despite the linearity, the relation is rather complicated. Since $P_{n+1+2s}^n(0) = 0$, $s \in \mathbb{N}_0$, we have that κ_n depends linearly on λ_{n+2s} , $s \in \mathbb{N}_0$, only. Furthermore, in our application the spherical variances λ_n are decreasing rapidly, and therefore the most important term when calculating κ_n is the first, which equals a constant times λ_n .

The covariance function in terms of the circular variances κ_n is given by

$$\text{Cov}(r(\theta_1, \pi/2), r(\theta_2, \pi/2)) = \sum_{n=2}^{\infty} \kappa_n \frac{1}{\pi} \cos(n(\theta_2 - \theta_1)),$$

and we have *stationarity on the circle* in the sense that the covariance between two points on the circle depends only on the angle between the points. This is of course a direct consequence of the stationarity on the sphere.

7. APPLICATION II: OBSERVING THE CENTRAL SECTION

Consider the ten central sections of neurons from the human hippocampus shown in Figure 2. The Fourier coefficients are obtained from discrete versions of the integrals in (6.1), where the standardized

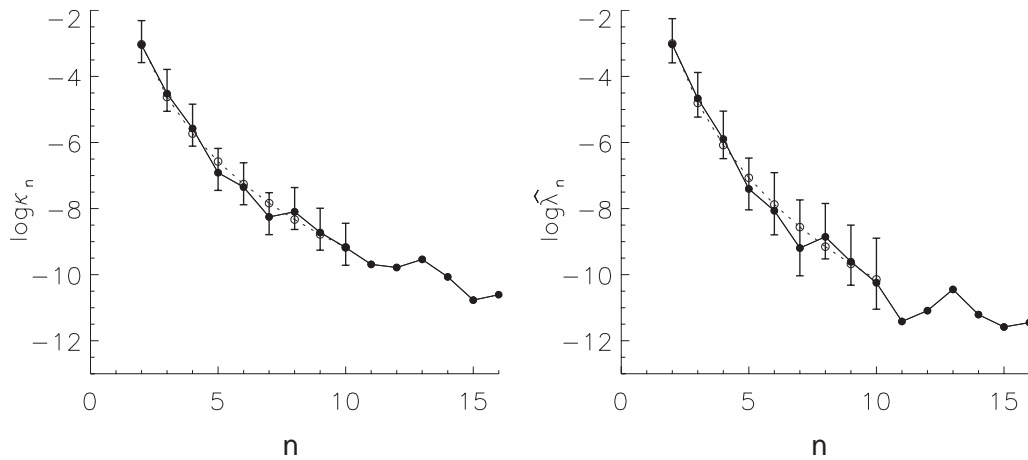


Fig. 7. Estimated circular (left) and spherical (right) log-variances of the stationary model (4.1; solid lines) and the regression model (4.3; dotted lines) for the 2D central sections. The error bars show the 95% confidence intervals under the stationary model.

radius-vector function is used. Estimates of the circular variances $\kappa_{n,k}$ for each of the ten objects $k = 1, \dots, 10 = K$ are calculated from the Fourier coefficients

$$\hat{\kappa}_{n,k} = \frac{(b_{n,k}^c)^2 + (b_{n,k}^s)^2}{2} \sim \kappa_{n,k} \chi^2(2)/2, \quad n \geq 2.$$

Suppose the objects are independent and identically distributed. Then the common variances κ_n are estimated by averaging the variances of the individual neurons

$$\hat{\kappa}_n = \frac{1}{K} \sum_{k=1}^K \hat{\kappa}_{n,k} \sim \kappa_n \chi^2(2K)/2K, \quad n \geq 2.$$

As in Section 5, the assumption of equal variances can be verified by a Bartlett test. Another possibility is to use the fact that a $\chi^2(2)/2$ distribution is an exponential distribution with mean one and consider the empirical survival function for each n . In the left-hand plot of Figure 7 the estimated circular log-variances are displayed. As in Section 5 we choose to truncate at $n^* = 10$ since the variances with indices larger than n^* are subject to noise due to digitization effects.

Using the linear relationship (6.2) it is possible to find approximate estimates of the spherical variances λ_n . The estimates are only approximate because the sum in (6.2) needs to be truncated. In the right-hand plot of Figure 7 the estimated spherical variances are displayed with a truncation at $l = 15$. Note the similarity of the decrease of the variances in Figures 5 and 7. Also, the relation between the spherical variances and the circular variances is similar to the relation between mean squares and variance components in ANOVA estimation of variance components from balanced data: see, for example Searle *et al.* (1992, Chapter 4). In particular, Satterthwaite's procedure (Satterthwaite, 1946) can be applied to approximate the distribution of the spherical variance estimates by $\chi^2(p)/p$ distributions, and thereby to determine confidence intervals for the spherical variances.

The linear relationship (6.2) also makes it possible to fit the (truncated) regression model (4.3). We fitted the model using maximum likelihood, and obtained the maximum likelihood estimates $(\hat{\alpha}, \hat{\beta}, \hat{p}) = (20.2, 0.9, 4.4)$. Figure 7 displays the circular and spherical log-variances under the fitted model. Carrying

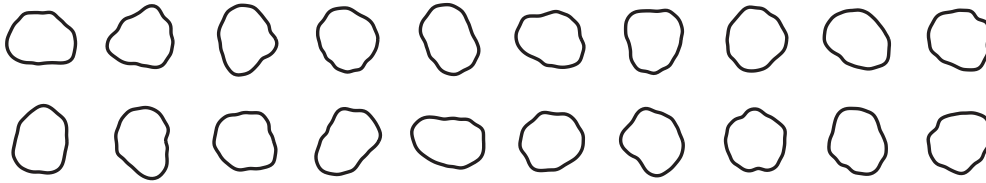


Fig. 8. Random samples from the regression model (4.3) with the fitted parameters from the ten central sections of neurons from the human hippocampus.

out a goodness of fit test of the regression model (4.3) under the model (4.1) assuming stationarity we obtain a likelihood ratio test statistic equal to 3.7 on 6 degrees of freedom. Under the $\chi^2(6)$ approximation of the test statistic the p -value is 0.72, and so we again judge the model to be reasonable. Fixing $p = 4$ as in application I we obtain the estimates $(\hat{\alpha}, \hat{\beta}) = (19.3, 2.1)$ with corresponding 95% confidence intervals [7.0, 31.6] for $\tilde{\alpha}$ and [0.61, 3.58] for β . Furthermore, the correlation between $\tilde{\alpha}$ and β is -0.09 . Note that these values agree well with the results obtained in application I.

In order to validate the central section regression model we again use a simulation study. Figure 8 shows random samples from the regression model (4.3), where the maximum likelihood estimates from the central sections were used for (α, β, p) . The random samples show similar shape variability as seen in the observed central sections in Figure 2.

8. DISCUSSION

In this paper we have analysed the spherical deformation model using two particular types of observations from an object, namely continuous observations of the surface or continuous observations of a central section. It should be emphasized that the spherical deformation model can also be analysed using a finite number of random or systematic observations of the surface. Suppose $r_i = r(\theta_i, \phi_i)$, $i = 1, \dots, n$, is a set of measurements of the radius-vector function of an object, and assume that the vector (r_1, \dots, r_n) follows a multivariate normal distribution with mean $\mu \in \mathbb{R}^n$ and $n \times n$ covariance matrix Σ . Under rotational symmetry (or stationarity) the entries $\Sigma_{ij} = \text{Cov}(r_i, r_j)$ of the covariance matrix Σ should only depend on the angle ψ_{ij} between the two vectors $\omega(\theta_i, \phi_i)$ and $\omega(\theta_j, \phi_j)$ on the unit sphere. Among the many possible families of covariance functions which could be proposed, this paper has mainly been concerned with the three-parameter regression model given by (4.2) and (4.3).

Prior to the analysis of a sample of 3D surfaces it is usually known if the objects can be viewed as small deformations of a sphere. In situations where the objects have one or more reference points, identifiable features or are elongated in a certain direction, the spherical deformation model is no longer suitable and other methods should be used. In Joshi *et al.* (1997) a stochastic model is introduced for representing the highly non-spherical shapes of cortical and hippocampal surfaces of macaque and human brains. First a cortical or hippocampal template \mathcal{M} is established. Second a complete orthonormal basis φ_n , $n \in \mathbb{N}$, of the template has to be determined. Joshi *et al.* (1997) suggest choosing the basis functions to correspond to eigenfunctions associated with a differential operator L , derived from thin elastic shell theory. Thus $L\varphi_n = \eta_n\varphi_n$, $n \in \mathbb{N}$, where η_n is the eigenvalue associated with the eigenfunction φ_n . A cortical or hippocampal surface is then determined by $\{x + U(x) : x \in \mathcal{M}\}$, where the Gaussian random field $\{U(x) : x \in \mathcal{M}\}$ is given by

$$U(x) = \sum_{n=1}^{\infty} a_n \varphi_n(x), \quad x \in \mathcal{M}.$$

Joshi *et al.* (1997) consider two models for the Gaussian random variables a_n , $n \in \mathbb{N}$. In both models the random variables are independent with zero means, but in the first the variances λ_n are chosen to be the inverse of the squared eigenvalues $1/\lambda_n = \eta_n^2$ whereas in the second the variances are estimated empirically from a sample of surfaces. The relation to the spherical deformation model is obtained by setting $\mathcal{M} = S^2$ and setting the operator L to be the Laplacian operator with eigenfunctions φ_n , $n \in \mathbb{N}$, equal to the spherical harmonics. In the spherical deformation model the independence assumption is reasonable on ground of rotational symmetry, but in general the assumption seems rather arbitrary and should be justified.

ACKNOWLEDGEMENT

Thanks go to Eva B. Vedel Jensen, John T. Kent and Jan Pedersen for valuable suggestions for improving the paper, and to Jens R. Nyengaard of the Stereological Research Laboratory at Aarhus University for providing the data. I would also like to thank the anonymous referee for many helpful comments.

APPENDIX: CHARACTERIZING THE CENTRE OF MASS

PROPOSITION Suppose $K \subset \mathbb{R}^3$ is a star-shaped object with respect to $z \in K$, and let $r(\theta, \phi; z)$ be the corresponding radius-vector function. If z is the centre of mass of K then

$$\int_0^{2\pi} \int_0^\pi r(\theta, \phi; z)^4 \varphi_1^m(\theta, \phi) \sin \phi \, d\phi \, d\theta = 0, \quad m = -1, 0, 1. \quad (\text{A.1})$$

Conversely, z is the centre of mass if (A.1) is fulfilled.

Proof. Let $F : [0, 2\pi] \times [0, \pi] \times [0, 1] \rightarrow \mathbb{R}^3$ be defined by

$$F(\theta, \phi, v) = z + vr(\theta, \phi; z)\omega(\theta, \phi).$$

Then F is onto K and elementary calculations show that the absolute value of the Jacobian determinant is $v^2 r(\theta, \phi; z)^3 \sin \phi$. Now if $x = (x_1, x_2, x_3) = F(v, \theta, \phi) \in K$ then

$$x_1 - z_1 = vr(\theta, \phi; z) \cos \theta \sin \phi = vr(\theta, \phi; z) \varphi_1^{-1}(\theta, \phi),$$

and by applying the transformation theorem we obtain

$$\begin{aligned} & \int_K (x_1 - z_1) \, dx_1 \, dx_2 \, dx_3 \\ &= \int_0^{2\pi} \int_0^\pi \int_0^1 vr(\theta, \phi; z) \varphi_1^{-1}(\theta, \phi) v^2 r(\theta, \phi; z)^3 \sin \phi \, dv \, d\phi \, d\theta, \end{aligned} \quad (\text{A.2})$$

which is zero if z is the centre of mass. The two remaining equations in (A.1) are obtained by replacing $(x_1 - z_1)$ in (A.2) by $(x_2 - z_2)$ and $(x_3 - z_3)$, and making similar calculations. \square

By making a first-order Taylor expansion we get

$$r(\theta, \phi)^4 \approx \bar{r}^4 + 4\bar{r}r(\theta, \phi),$$

and it follows from the proposition that $a_1^m \approx 0$, $m = -1, 0, 1$ if z is close to the centre of mass. The Taylor expansion is adequate when the objects are small deformations of a sphere.

REFERENCES

- AMARAL, D. G. AND WITTER, M. P. (1989). The three-dimensional organization of the hippocampal formation: a review of anatomical data. *Neuroscience* **31**, 571–591.
- GRENANDER, U. AND MILLER, M. I. (1994). Representations of knowledge in complex systems (with discussion). *Journal of the Royal Statistical Society, Series B*, **56**, 549–603.
- GRENANDER, U. AND MILLER, M. I. (1998). Computational anatomy: An emerging discipline. *Quarterly of Applied Mathematics* **5**, 617–694.
- HOBOLTH, A., KENT, J. T. AND DRYDEN, I. L. (2002). On the relation between edge and vertex modelling in shape analysis. *Scandinavian Journal of Statistics* **29**, 355–374.
- HOBOLTH, A., PEDERSEN, J. AND JENSEN, E. B. V. (2003). A continuous parametric shape model. *Ann. Inst. Stat. Math.* **55**, To appear.
- JOSHI, S. C., MILLER, M. I. AND GRENANDER, U. (1997). On the Geometry and Shape of Brain Submanifolds. *International Journal of Pattern Recognition and Artificial Intelligence* **11**, 1317–1343.
- KENT, J. T., DRYDEN, I. L. AND ANDERSON, C. R. (2000). Using circulant symmetry to model featureless objects. *Biometrika* **87**, 527–544.
- LESTREL, P. E. (ed.) (1997). *Fourier Descriptors and their Applications in Biology*. New York: Cambridge University Press.
- MILLER, M. I., JOSHI, S., MAFFITT, D. R., McNALLY, J. G. AND GRENANDER, U. (1994). Membranes, mitochondria and amoeba: shape models. In Mardia, K. (ed.), *Advances in Applied Statistics*, vol. II. Abingdon: Carfax, pp. 141–163.
- MÜLLER, C. (1966). *Spherical Harmonics*. Berlin: Springer.
- SATTERTHWAITE, F. E. (1946). An approximate distribution of variance components. *Biometrics Bull.* **2**, 110–114.
- SEARLE, S. R., CASELLA, G. AND MCCULLOCH, C. E. (1992). *Variance Components*. New York: Wiley.
- STEIN, M. L. (1999). *Interpolation of Spatial Data*. New York: Springer.
- WEST, M. J. (1994). Advances in the study of age-related neuron loss. *The Neurosciences* **6**, 1–9.
- WEST, M. J., COLEMAN, P. D., FLOOD, D. G. AND TRONCOSO, J. C. (1994). Differences in the pattern of hippocampal neuronal loss in normal aging and Alzheimer's disease. *The Lancet*, **344**, 769–772.

[Received February 19, 2002; first revision September 9, 2002; second revision February 17, 2003;
accepted for publication February 21, 2003]